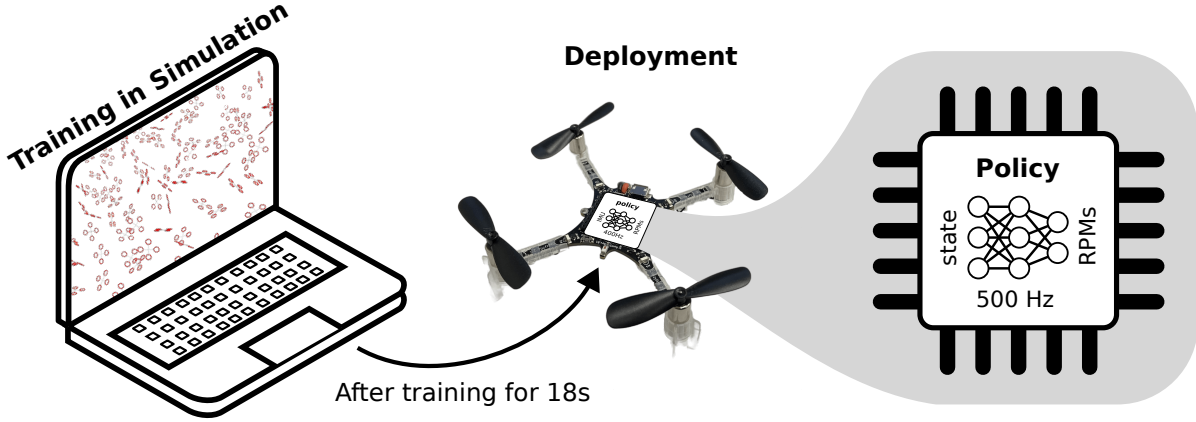


Learning to Fly in Seconds

Jonas Eschmann^{1,2}, Dario Albani², and Giuseppe Loianno¹



Abstract—Learning-based methods, particularly Reinforcement Learning (RL), hold great promise for streamlining deployment, enhancing performance, and achieving generalization in the control of autonomous multirotor aerial vehicles. Deep RL has been able to control complex systems with impressive fidelity and agility in simulation but the simulation-to-reality transfer often brings a hard-to-bridge reality gap. Moreover, RL is commonly plagued by prohibitively long training times. In this work, we propose a novel asymmetric actor-critic-based architecture coupled with a highly reliable RL-based training paradigm for end-to-end quadrotor control. We show how curriculum learning and a highly optimized simulator enhance sample complexity and lead to fast training times. To precisely discuss the challenges related to low-level/end-to-end multirotor control, we also introduce a taxonomy that classifies the existing levels of control abstractions as well as non-linearities and domain parameters. Our framework enables Simulation-to-Reality (Sim2Real) transfer for direct Revolutions Per Minute (RPM) control after only 18 seconds of training on a consumer-grade laptop as well as its deployment on microcontrollers to control a multirotor under real-time guarantees. Finally, our solution exhibits competitive performance in trajectory tracking, as demonstrated through various experimental comparisons with existing state-of-the-art control solutions using a real Crazyflie nano quadrotor. We open source the code including a very fast multirotor dynamics simulator that can simulate about 5 months of flight per second on a laptop GPU. The fast training times and deployment to a cheap, off-the-shelf quadrotor lower the barriers to entry and help democratize the research and development of these systems.

SUPPLEMENTARY MATERIAL

Video: <https://youtu.be/NRD43ZA1D-4>

Code: <https://github.com/arplaboratory/learning-to-fly>

Parameters: <https://github.com/{...}/parameters.pdf>

¹The authors are with the New York University, Tandon School of Engineering, Brooklyn, NY 11201, USA. email: {jonas.eschmann, loiannog}@nyu.edu.

²The authors are with the Autonomous Robotics Research Center, Technology Innovation Institute, Abu Dhabi, UAE. email: {jonas.eschmann, dario.albani}@tii.ae.

Giuseppe Loianno serves as consultant for the Technology Innovation Institute. This arrangement has been reviewed and approved by the New York University in accordance with its policy on objectivity in research.

I. INTRODUCTION

With the availability of cheap Commercial Off-The-Shelf (COTS) gyroscopes and accelerometers that are implemented as Microelectromechanical Systems (MEMS), the large-scale production of cheap Unmanned Aerial Vehicles (UAVs), particularly quadrotors, became viable. Bearing Vertical Take-Off and Landing (VTOL) as well as hovering capabilities a myriad of use cases, such as search and rescue, infrastructure inspection, or package delivery emerged. Leveraging classical, cascaded control hierarchies, multirotors are able to perform a variety of tasks. However, these control approaches require domain expertise and engineering to be adapted to new platforms and use cases. At the same time, the recent developments in machine learning and particularly the success of deep learning for supervised tasks like image classification [1], [2], raise the question if these learning-based capabilities could be transferred to quadrotor control. In contrast to supervised learning, (multirotor) control is a decision-making problem that can be phrased as a Markov Decision Process (MDP) where labels usually do not directly exist. To solve MDPs, RL has been employed to train policies for complex continuous control problems in simulation [3]–[6]. However, while the results attained in simulation are impressive, most of the downstream use cases involving real robots show limited performance. This is mainly due to model inaccuracies, partial observation of the state, observation and action noise, and other disturbances. It is often assumed that without extra measures like domain randomization [7]–[9] policies can not be successfully transferred to real robots but in our experiments, we demonstrate this to be possible even for complex systems like quadrotors. Furthermore, to better highlight the challenges and clarify the scope of true end-to-end control, we describe the different levels of quadrotor dynamics and control by developing a taxonomy to categorize related work. We argue that the abstractions in classic control stacks introduce information

loss (e.g., actuator constraints in differential flatness-based control) and constrain the expressivity of the control policy. Due to Bellman’s Principle of Optimality (BPO), the optimal policy for a decision/control problem can be represented as a function mapping from states/observations to actions. Hence, in theory, the optimal policy can be expressed as a neural network which in the limit is a general function approximator [10]. Compared to general function approximators, classical control stacks (based on multi-level abstractions) have limited expressivity and can not necessarily represent the optimal policy, especially when accounting for evermore (non-linear) factors in the simulation. Optimization-based controllers can circumvent this limitation but are usually too computationally expensive to run end-to-end control under hard real-time constraints inside microcontrollers. Hence, we believe it can be desirable to design and train an end-to-end controller using RL, directly mapping the quadrotor state to RPM outputs.

We observe that the end-to-end control of quadrotors using state-of-the-art deep RL techniques (especially using off-policy RL) is not well explored and documented. It is particularly unclear which level of performance end-to-end policies can achieve compared to classic controllers when deployed directly on a real quadrotor under real-time constraints. With this work, we aim to push the boundaries of deep RL-based end-to-end quadrotor control and present the following contributions

- **RL-based controller design:** We propose a novel asymmetric actor-critic-based architecture coupled with a highly reliable training paradigm for end-to-end quadrotor control. The proposed training paradigm takes advantage of the ground truth available in the simulator while explicitly accounting for the partial observability of the real system using an action history.
- **Best sample complexity:** We devise a curriculum that gradually increases the penalties in the reward function leading to better sample complexity and more reliable policies. We show the benefit of the components in our proposed training paradigm by conducting an extensive ablation study containing 300 real-world trajectories across different configurations, seeds and tasks. In contrast to existing works, our training setup uses off-policy RL and we demonstrate the training of an end-to-end quadrotor control policy using the fewest number of environment interactions reported.
- **Fastest training time:** By implementing a highly optimized simulator, we demonstrate the fastest training of an end-to-end quadrotor control policy that can be transferred to a real system.
- **Sim2Real:** We conduct extensive experiments including more than 300 flights across configurations, seeds and tasks to test the Sim2Real transfer of end-to-end policies for direct RPM control. We show that training a position controller using our setup generalizes to other tasks like (agile) trajectory tracking.
- **Open Source:** We open-source our setup to facilitate

research, enabling everyone with a consumer-grade laptop to train and deploy state-of-the-art quadrotor control policies in a matter of seconds, greatly reducing the barriers to entry in this research area.

II. TAXONOMY OF MULTIROTOR DYNAMICS AND CONTROL

In the following, we introduce a taxonomy classifying the different abstraction levels in multirotor dynamics and control. We believe this taxonomy to be beneficial to the discussion as it allows for the precise categorization of different controllers, particularly those that we analyze in the related work (see Section III). Furthermore, it explicitly exposes at which levels non-linearities and domain parameters exert an influence on the motion of multirotors. We list the different control levels based on the order of the system when expressed in terms of a flat state. The taxonomy shown in Fig. 1 is expressed from the perspective of a position controller and each subsequent level denotes a lower level of control inputs. The sub-bullets denote non-linear transformations that allow expressing the dynamical system using different inputs. These transformations are not only challenging because of the non-linearity they bear but also due to the additional system/domain parameters they might introduce (marked in square brackets). It is worth noting that every layer incorporates an additional level of indirection, manifesting in the form of integrators. The lower the input level to the system is chosen, the more detached the effect on the higher level (e.g., the position) is from the cause (e.g., RPM setpoints). For controllers on the lowest levels, the cause-effect relationship traverses through up to five orders of integration and multiple non-linear transformations that are dependent on system parameters. We would like to highlight that **3.1 Angular rate & thrust** inputs are commonly

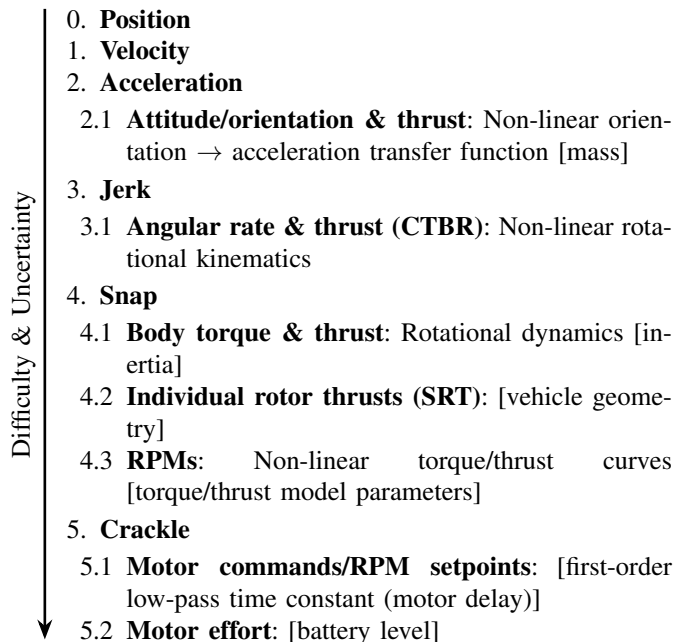


Fig. 1: Taxonomy of multirotor dynamics and control.

referred to as “low-level” commands but from the taxonomy, we can see that there is only one domain parameter (mass) and otherwise just the rotational kinematics of a rigid body. Alternatively, **3.1 Angular rate & thrust** inputs are also commonly referred to as Collective Thrust and Body Rates (CTBR) inputs. Compared to the CTBR level, the reality gap and complexity of the system greatly increases towards the lowest levels like **5.1 Motor commands/RPM setpoints** which is the level of control used in this work. The high order of integration between inputs and the desired output (position) poses a great challenge for RL algorithms because the high-frequency exploratory actions (from ϵ -greedy-like exploration schemes) are already suppressed in the early layers and hence lead to high-sample complexity and unreliable training behavior. In our proposed architecture, we overcome this challenge by using a combination of off-policy RL, curriculum learning, and by scheduling the exploration noise. From Fig. 1, we can observe that the complexity of the control problem, as well as the size of the reality gap, follows a superlinear scaling where most of the non-linear dynamics and system parameters can be found in the lower levels.

III. RELATED WORKS

Simulators. In the past, a large number of general robotics and specifically quadrotor simulators have been proposed. Many of these focus on visual fidelity and photo-realistic reproduction of the environment (e.g., to enable realistic RGB camera perception) [11]–[14]. Others, as the one presented in this work, focus on the accurate implementation of quadrotor dynamics [13]–[16]. Among the referenced simulators, Flightmare [13] is the most related because it emphasizes the simulation speed of the quadrotor dynamics for the sake of RL. Our simulator also focuses on fast dynamics but since we are concerned with low-level control we just provide a basic User Interface (UI) instead of the photo-realism that is offered by other simulators.

Reinforcement learning for quadrotor control. As described in Section II, it is usually easier to learn controllers on the higher levels, especially for Sim2Real transfer. Hence, a lot of work that focuses on downstream tasks has been using CTBR and higher-level control inputs to train RL based agents. The use of velocity commands has been particularly common [17]–[22]. Fewer works also use orientation level commands [23], [24] or angular rate commands (CTBR) [22], [25]–[27]. The latter is usually used when increased agility is required (e.g., for acrobatics, racing, or flying through a narrow gap).

To use the quadrotor dynamic’s full potential, the focus has been shifting to training agents outputting individual rotor thrusts (also referred to as Single Rotor Thrusts (SRT)) [22], [28]–[31]. The authors in [32] even go lower-level, training a controller outputting RPM. These represent the works that are closely related to our proposed solution. In the following, we will discuss their similarities and differences. One of the earliest demonstrations of the successful application of deep RL for quadrotor control has been presented in

| Publication | Level | Time | Samples |
|-------------|---------|------------|-------------------------------------|
| 2019 [33] | 5.1 | 9 h | 10×10^6 |
| 2019 [29] | 4.3/5.1 | N/A | 168×10^6 |
| 2020 [30] | 4.3 | N/A | 10×10^6 |
| 2021 [31] | 4.3 | ~ 2 h | N/A |
| 2021 [25] | 2.1 | 27 m | 1×10^6 |
| 2023 [27] | 3.1 | 21 m | N/A |
| Ours | 5.1 | 18 s | 0.3×10^6 |

TABLE I: Training times.

[28]. The authors train a position controller that outputs individual rotor thrusts but in contrast to our approach, they are using a complex training procedure (exploration scheme) that requires a resettable simulator and drives up the sample complexity to more than 100 million environment steps. Additionally, they do not take into account rotor delays and their code is not available. In [29], the authors apply domain randomization to transfer a policy that outputs SRT to different quadrotors but they require knowledge about the particular thrust-to-weight ratio and thrust limits. In comparison, our approach demonstrates Sim2Real transfer without domain randomization and without modifications to the state estimation in the firmware as well as much faster training times (comparison in Table I). In [22] the authors perform a benchmark of training controllers outputting velocity, CTBR and SRT commands but in contrast to our work they did not manage to transfer the low-level controller (SRT) to the real world. Moreover, in all of the aforementioned works as well as in [22], [30], [31], SRT control outputs are used which simplify the learning problem by not exposing the agent to the non-linear $\text{RPM} \leftrightarrow \text{thrust}$ relationship. Furthermore, in the latter three cases, the code is not published for independent replication and benchmarking. Lastly in [32], RPM outputs are used but rather than cutting out lower-level controls to simplify the learning problem as commonly done and described in Section II, they discard the higher-level control and take CTBR as input from a high-level controller. Their work focuses on the adaptability and transferability between different quadrotors and hence the decision about the architecture is also aligned with our earlier observation in Section II that most of the dynamic parameters are at the lower-level control where the adaptation takes place in their work. In contrast to all the most related work which rely on on-policy, policy gradient RL algorithms (particularly Proximal Policy Optimization (PPO)), we use Twin Delayed Deep Deterministic policy gradient (TD3), an off-policy RL algorithm which offers better sample complexity and helps us achieve very fast wall-clock training times.

IV. METHODOLOGY

To be able to take full advantage of the capabilities of the robot, we phrase our control problem as an MDP where the policy directly maps states to motor commands in the form of RPMs. We select quaternions to represent orientation as they are a compact and global representation. However, for the observations fed into the actor and critic, we convert them to rotation matrices to remove the ambiguity stemming from the

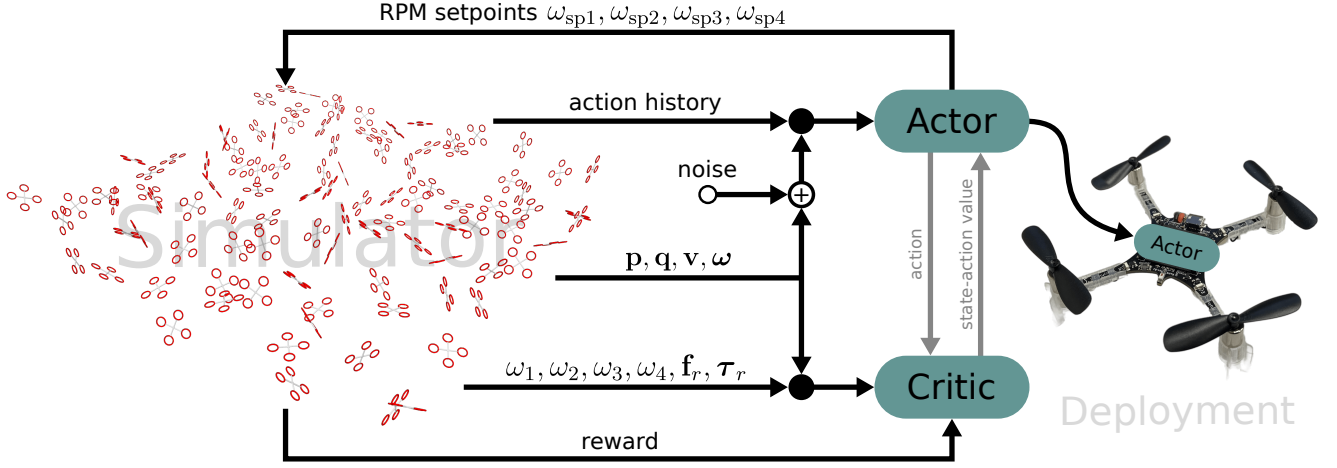


Fig. 2: Overview of the training and inference setup with a view of the simulator UI (left).

quaternion’s double coverage of the space of rotations. Since we model the motors as a first-order low-pass filter, RPMs are also part of the state. This makes the state 17 dimensional with the following structure $\mathbf{s} = \{\mathbf{p}, \mathbf{q}, \mathbf{v}, \boldsymbol{\omega}, \boldsymbol{\omega}_m\}$, consisting of position, orientation, linear and angular velocity and motor speeds respectively.

On real platforms, motor speeds are usually not observable and RPM setpoints are fed to the Electronic Speed Controller (ESC) in a feed-forward, one-way fashion through Pulse-Width Modulation (PWM). Hence, we implement an asymmetric actor-critic scheme [34], where the critic, being only required during training, has access to privileged information from the simulator. In particular, we let the critic access the RPMs and a random force \mathbf{f}_r and torque $\boldsymbol{\tau}_r$ disturbance that are sampled at the beginning of each episode to increase the robustness of the trained policies. Hence, the privileged observations of the critic are represented by a 28 dimensional vector $\mathbf{o}_c = \{\mathbf{p}, \mathbf{R}, \mathbf{v}, \boldsymbol{\omega}, \boldsymbol{\omega}_m, \mathbf{f}_r, \boldsymbol{\tau}_r\}$ consisting of position, orientation, linear velocity, angular velocity, rotor speeds, force disturbance, and torque disturbance respectively.

We also notice that the delay in the step-response on quadrotors is significant and caused by their low-pass behavior. This behavior also strongly impacts the dynamics of the 27 g nano quadrotor (Crazyflie) used in this work. Common values for the RC equivalent time constant ($1 - e^{-1} \approx 63\%$ step response) are between 0.05 s and 0.25 s. We empirically find 0.15 s to be suitable for Sim2Real transfer which is also supported by the manufacturers measurements¹. These delays are significantly larger than the usual control interval of low-level controllers which usually run at around hundreds of Hz. Therefore, these delays lead to actions only impacting the state after 5 to 25 control steps. To mitigate this large level of partial observability, we add a history of control actions to the actor’s observation. The action history is a proprioceptive measurement that can be trivially implemented in software

on any real-world platform without requiring additional hardware (in contrast to direct RPM feedback measurements). Therefore, the actor’s observations are $18 + N_H \cdot 4$ dimensional, where N_H is the length of the action history, and are defined as follows: $\mathbf{o}_a = \{\mathbf{p}, \mathbf{R}, \mathbf{v}, \boldsymbol{\omega}, \mathbf{H}\}$ with \mathbf{H} being the action history.

While the critic observes the ground truth state, the actor’s observations are additionally perturbed using observation noise to account for imperfections in the sensors (the scale of the noise components is described with all other parameters in the supplementary material). The actions consist of the RPM setpoints as $\mathbf{a} = \{\omega_{sp1}, \omega_{sp2}, \omega_{sp3}, \omega_{sp4}\}$ which places our policy/controller on the lowest order (level 5.1) of the taxonomy described in Section II.

For the initial state distribution, we sample from a diverse set of positions, orientations, linear and angular velocities as well as rotor speeds. We use a negative squared cost with an additive constant incentivizing survival to mitigate the “learning to terminate” problem [35]

$$r(s, a, s') = -C_{rp}\|\mathbf{p}\|_2^2 - C_{rq}(1 - q_w^2) - C_{rv}\|\mathbf{v}\|_2^2 - C_{r\omega}\|\boldsymbol{\omega}\|_2^2 - C_{ra}\|\mathbf{a}\|_2^2 - C_{rab}\|\mathbf{a}\|_2^2 + C_{rs}.$$

The values of the constants C_* are supplied in the supplementary material. Additionally, we find that a simple curriculum that is transitioning from an initial set of constants $C_{init,*}$ to a more restrictive $C_{target,*}$ (punishing position errors and particularly control actions more harshly) benefits the sample complexity and Sim2Real transfer (as described in Section V). Every 100 000 steps the weights are adjusted by multiplying them by the C_{p*} factors described in the supplementary material until they reach the $C_{target,*}$ values, where they remain constant. We also decay the exploration noise using the same exponential scheme as in the curriculum of the reward function.

We would also like to highlight that we train a position controller, not merely a stabilizing controller that only works around a particular state. The goal of our position controller is to return to the origin point with zero linear velocity from

¹Crazyflie motor step response: <https://web.archive.org/web/20220309092320/https://www.bitcraze.io/wp-content/uploads/2015/02/M1-step-responses.png>

any initial conditions (within reasonable bounds described in the parameters in the supplementary material). Hence, we train a policy that can go to any position or velocity setpoint by shifting the current position and velocity (so there is no need to apply goal-conditioned RL). For stable behavior, the position and velocity errors induced by the shifted setpoints should not exceed the errors seen during training which can easily be accommodated for by clipping.

To facilitate fast training times we implement a highly optimized simulator for multirotor dynamics. A sample view of the interface is shown in Fig. 2 (left). By leveraging C++ template metaprogramming the simulation code can be highly optimized by the compiler and can be tightly integrated into the RLtools [36] deep RL framework.

V. EXPERIMENTAL SETUP

Simulation. We run our multirotor dynamics simulator on a Nvidia T2000 laptop GPU and attain 1284 million steps/s. To reach this level of performance, 64 blocks of 128 threads are each executing the forward dynamics in parallel. This amounts to 8192 environments in total which are run for 1 000 000 steps each. The required execution time of the GPU kernel is 6380 ms amounting to 1284 million steps/s. At a simulation frequency of 100 Hz this is about 5 months of simulated flight per second. Compared to Flightmare [13] which is the state of the art in terms of dynamics simulation speed with a reported frequency of 200 000 steps/s on a laptop, our simulation is about $6420\times$ faster.

Training. Leveraging the training setup described in Section IV and using the RLtools RL framework [36], we train a low-level quadrotor control policy. Fig. 3 shows the learning curve in terms of the returns (sum of rewards per episode). Purely looking at the reward/returns, it is hard to judge the level of flying capabilities of a particular policy because it is highly dependent on the reward function formulation. We believe the episode length is a more understandable measure than the return because if the agent crashes or flies away from a tight box around the origin, the episode is terminated. Hence, from Fig. 4 we can see that after about 300 000 steps (total number of interactions with the environment) or 18 s of training on a 2020 MacBook Pro, the policy has learned to fly relatively reliably. In comparison to related work (listed in Table I) our approach is substantially faster and requires an order of magnitude less samples when compared to learned policies on a similar level of control outputs.

We investigate the 50 differently seeded training runs by selecting the 5 seeds with the worst cumulative number of steps over the whole training run (area under the curve) shown in Fig. 4. We notice that even the worst 5 runs learn to fly rapidly. This shows the remarkable reliability of our training approach which is not commonly expected from RL training pipelines (e.g., in [29] the authors state that cherry-picking across many seeds is required to find a policy that can fly). This remarkable level of reliability is also confirmed by real-world experiments that are described in the following.

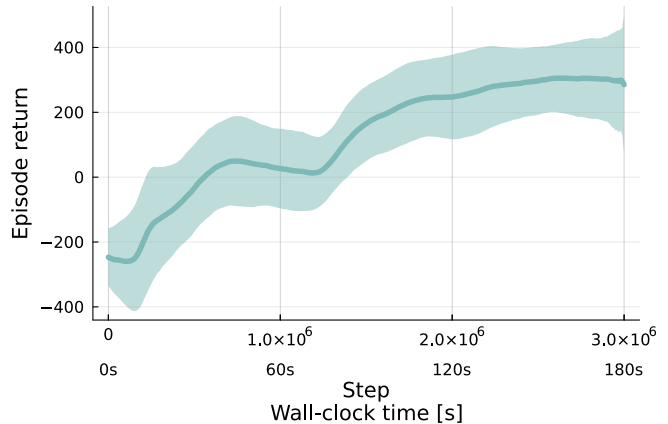


Fig. 3: Episode return (μ and σ over 50 runs with different initial seeds).

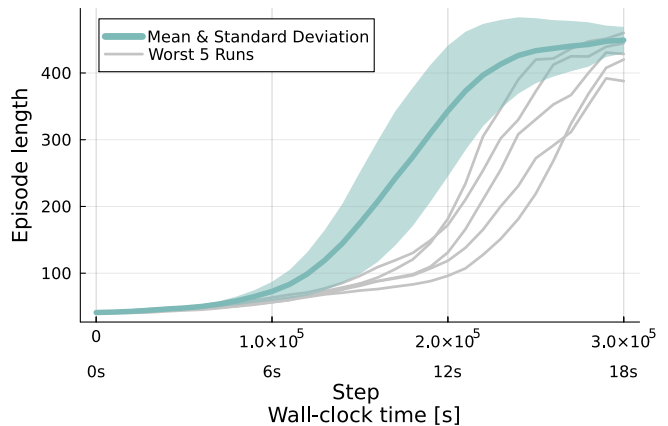


Fig. 4: Episode lengths (μ and σ over 50 runs with different initial seeds). Note, compared to Fig. 3 the horizontal axis is zoomed in to highlight the initial phase.

VI. RESULTS

Ablation study. To show the impact of the different components of the training setup (as shown in Fig. 2) on the performance during training and real-world deployment, we conduct a large-scale ablation study and present the results in Table II. We train each configuration for up to 3 000 000 steps using 50 different initial seeds each. Figs. 3 and 4 are generated from the 50 runs of the baseline configuration (containing all components). Furthermore, we execute the resulting policy after 300 000 and 3 000 000 steps of training using the first 10 different seeds of each configuration on a real Crazyflie quadrotor. We manually terminate the position control episodes after 20 s of flying because in our experience, at this level, policies can fly without crashing until the battery runs out. In the case of the trajectory tracking task, we complete 4 subsequent cycles or report a failed attempt if the quadrotor crashes beforehand. We report the mean and median as well as the minimum of the position error across the 10 runs/seeds. The minimum positional error is a particularly interesting metric because it corresponds to cherry-picking which is common in related works (e.g., [29]). We would like to note that turning off the rotor delay also implies turning

| Task | Training (Simulation) | | | | Inference (Real World) | | | | | | | | | | | |
|-------------------------|-----------------------|-------------|------------|------------|------------------------|-------------|------------------|------------------|---------------------|-------------|------------------|------------------|--------------|-------------|------------------|------------------|
| | Position Control | | | | Position Control | | | | Trajectory Tracking | | | | | | | |
| | 300 000 | | 3 000 000 | | 300 000 | | | | 3 000 000 | | | | | | | |
| Checkpoint [steps] | | | | | | | | | | | | | | | | |
| Ablation | N | R | N | R | # | \bar{e} | e_{med} | e_{min} | # | \bar{e} | e_{med} | e_{min} | # | \bar{e} | e_{med} | e_{min} |
| All Components | 398 | -335 | 368 | 302 | 10/10 | 0.26 | 0.24 | 0.1 | 10/10 | 0.34 | 0.38 | 0.18 | 10/10 | 0.27 | 0.26 | 0.21 |
| Observation Noise | 392 | -346 | 369 | 313 | 10/10 | 0.26 | 0.27 | 0.1 | 8/10 | 0.33 | 0.31 | 0.23 | 10/10 | 0.21 | 0.21 | 0.16 |
| Reward Recalculation | 391 | -455 | 394 | 319 | 9/10 | 0.24 | 0.15 | 0.07 | 9/10 | 0.34 | 0.3 | 0.25 | 7/10 | 0.22 | 0.22 | 0.2 |
| Exploration Noise Decay | 398 | -335 | 363 | 303 | 9/10 | 0.25 | 0.22 | 0.08 | 8/10 | 0.31 | 0.3 | 0.19 | 10/10 | 0.21 | 0.18 | 0.15 |
| Disturbances | 404 | -310 | 375 | 291 | 9/10 | 0.28 | 0.27 | 0.08 | 8/10 | 0.33 | 0.32 | 0.21 | 10/10 | 0.21 | 0.21 | 0.17 |
| Asymmetric Actor-Critic | 186 | -305 | 429 | 272 | 6/10 | 0.28 | 0.29 | 0.08 | 4/10 | 0.4 | 0.34 | 0.32 | 9/10 | 0.25 | 0.26 | 0.19 |
| Action History | 138 | -332 | 296 | 27 | 5/10 | 1.18 | 1.41 | 0.25 | 5/10 | 0.63 | 0.6 | 0.25 | 0/10 | ∞ | ∞ | ∞ |
| Curriculum | 64 | -200 | 384 | 180 | 1/10 | 0.18 | 0.18 | 0.18 | 1/10 | 0.23 | 0.23 | 0.23 | 9/10 | 0.2 | 0.2 | 0.15 |
| Rotor Delay | 46 | -207 | 44 | -195 | 0/10 | ∞ | ∞ | ∞ | 0/10 | ∞ | ∞ | ∞ | 0/10 | ∞ | ∞ | ∞ |
| AAC & Curriculum | 44 | -178 | 383 | 17 | 0/10 | ∞ | ∞ | ∞ | 0/10 | ∞ | ∞ | ∞ | 2/10 | 0.26 | 0.26 | 0.23 |

TABLE II: Ablation study: Removing different components from the baseline (which includes all the components). The *Ablation* column describes the component that is removed. Returns R and number of steps per episode (N) are mean over 50 training runs with different seeds each. The mean(\bar{e})/median(e_{med})/minimum(e_{min}) of the position error (in the xy-plane) are statistics over 10 flights of the real quadrotor with policies from different seeds each (no cherry-picking, seeds are the first 10 of the 50 trained in simulation). The # column shows the number of successful flights (without crashing). For the trajectory tracking task we use the figure-eight trajectory shown in Fig. 5b with an interval of $T = 5.5$ s. For each metric, the best value is marked in bold. The best values of the real-world tests are awarded provided that at least 5/10 of the runs/seeds of a particular configuration are successful for each of the three tests.

off the action history (as there is no partial observability of the true RPM anymore). In the ablation of the asymmetric actor-critic, the critic, like the actor, receives action history observations. Since the curriculum entails changes in the reward function and we apply reward recalculation of all rewards in the replay buffer after each modification of the reward function, we also ablate the setup without reward recalculation. Note that the configurations differ drastically in the added/removed complexity. The components observation noise, reward recalculation, exploration noise decay, and disturbances are relatively minor changes to the baseline, while the asymmetric actor-critic structure, action history as well as rotor delay, and the curriculum are more drastic modifications in terms of complexity of the implementation as well as the expected impact on the training behavior.

From the results in Table II, we can see that overall (and particularly when executed on the real system) the baseline is the most reliable with no crashes in any of the tasks/seed combinations. In general, we can observe a trend that removing the smaller modifications still yields reliable policies (early during the training as well as after convergence). In contrast, when removing the more complex components, we can see a more pronounced drop in reliability as well as tracking performance. Here, we can observe that the curriculum indeed strongly impacts the training speed. Without the curriculum, the policies are not able to fly early on while after convergence they reach a comparable performance to the baseline. We can observe a similar behavior when removing the Asymmetric Actor-Critic (AAC) and hence also ablate removing both, the asymmetric actor-critic and the curriculum and find that the training takes considerably longer and even after 3 000 000 steps most of the policies are crashing. As deduced from first principles, we can also confirm that training without

simulating the rotor delay leads to no usable policy. When simulating the rotor delays but not including the action history we can still see a considerable drop in reliability and positional accuracy, particularly after 3 000 000 steps where the policy seems to be overfitting the system dynamics. This validates the need for an action history to account for the partial observability in our training setup. When taking into account the average episode lengths and returns achieved by the different configurations during training in simulation we can only observe a loose correlation between simulation and real-world performance. As described earlier, the episode lengths appear to be a better gauge for the real-world performance as well.

We conclude that overall the baseline configuration with all components and the configurations with minor ablations yield the best performance when taking into account the speed of training (sample complexity) and position error. We observe that the baseline configuration yields the most reliable policies at all stages and anecdotally is also most robust with respect to e.g. turbulent wind (cf. the supplementary video). For trajectory tracking, after 3 000 000 steps in particular, we find that the configuration without exploration noise gives the lowest tracking error among the tested seeds and hence chose it for the trajectory tracking experiments in the next section. Overall, we observe multiple reliable configurations that can fly as long as the battery lasts, which is a big improvement over e.g. [37] where RL-based control was able to fly Crazyflies for only up to 6 s. Compared to [29] we do not require a modification of the firmware (adjusting the gyroscope filter), complex motor noise (Ornstein-Uhlenbeck process) and cherry-picking seeds/policies.

Trajectory tracking. In addition, even though we train a position controller, we find that the resulting policies can track trajectories like the Lissajous in Fig. 5 when

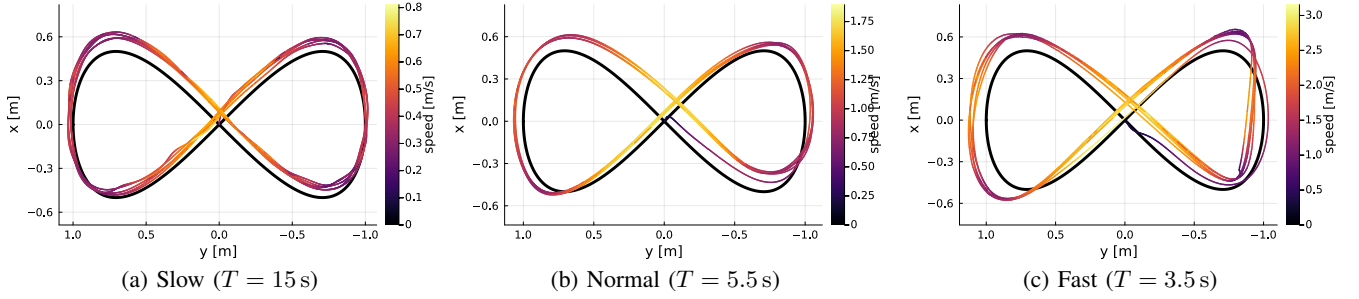


Fig. 5: Real-world tracking of a Lissajous trajectory with different cycle times (reference trajectory in black).

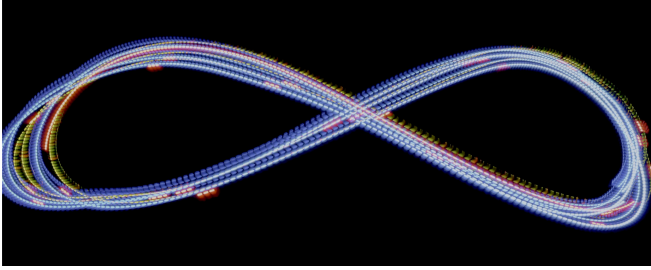


Fig. 6: Long exposure photo of the real-world tracking of a Lissajous trajectory with a 5.5 s cycle time.

| Interval | Slow (15 s) | | Normal (5.5 s) | | Fast (3.5 s) | |
|----------------|-------------|----------------|----------------|----------------|--------------|----------------|
| Controller | \bar{e} | \bar{e}_{xy} | \bar{e} | \bar{e}_{xy} | \bar{e} | \bar{e}_{xy} |
| PID | 0.23 | 0.22 | 0.72 | 0.72 | 0.88 | 0.87 |
| Geometric [38] | 0.06 | 0.04 | 0.16 | 0.16 | 0.36 | 0.36 |
| Nonlinear [39] | 0.29 | 0.11 | 0.38 | 0.32 | ∞ | ∞ |
| INDI [40] | 0.21 | 0.21 | 1.13 | 1.13 | 1.04 | 1.04 |
| Ours | 0.08 | 0.08 | 0.17 | 0.15 | 0.24 | 0.22 |

TABLE III: Real-world trajectory tracking error \bar{e} (Root-Mean-Square Error (RMSE) including z in meter) and \bar{e}_{xy} (RMSE excluding z in meter) when tracking the Lissajous trajectory in Fig. 5 using different controllers.

deployed on the real quadrotor. We test the tracking performance using a figure-eight Lissajous trajectory $\mathbf{p}(t) = [\cos(2\pi t/T) \ \sin(4\pi t/T)/2 \ \text{const}]^\top$ with varying cycle times T and show the tracking performance in Fig. 5. We conduct the trajectory tracking experiments in a flying space of $10 \times 6 \times 4 \text{ m}^3$ at the Agile Robotics and Perception Lab (ARPL) at New York University (equipped with a Vicon motion capturing system). We can see that our trained policy is able to track even agile trajectories like in Fig. 5c where it reaches up to 3 m s^{-1} and accelerations of up to 0.9 g . In Fig. 6, we show a long-exposure photo of the trajectory in Fig. 5b being tracked by one of our policies.

We execute the same trajectory using different types of classical controllers: Proportional–Integral–Derivative (PID), geometric [38], nonlinear [39] and Incremental Non-Linear Dynamic Inversion (INDI) [40]. We report the results in Table III and find that the geometric controller [38] gives the lowest tracking error among these classical controllers because, like our approach, it can take advantage not only of the position but also the velocity reference of the tra-

jectory. The nonlinear controller [39] also uses the velocity reference but performs worse on low speeds and crashes in the fast setting. Compared to the other controllers our learned controller directly outputs RPMs and hence does not take advantage of the battery voltage compensation, hence we also report the RMSE without the z component. Using the slow trajectory, the geometric controller [38] performs better than our policy which we attribute to its integral part which can help it to reduce the steady state error. Our policy does not have memory (which the integral part can be seen as) which it could use to reduce the steady-state position error. In the case of the normal-speed trajectory our policy is roughly on par with the geometric controller [38] and when moving to even more agile trajectories the performance gap inverts and our policy achieves lower error compared to [38]. Anecdotally, we also find that the geometric controller (using the default configuration in the Crazyflie) is very sensitive to position and velocity errors and is unstable during the takeoff. In contrast, most of our policies are robust towards higher position and velocity errors and hence also manage to take off as a response to a step function in z .

VII. CONCLUSION

In this work, we presented an unprecedentedly fast RL architecture for quadrotor control that directly outputs RPMs and can be trained to fly a real quadrotor in 18 s on consumer-grade laptops. The approach directly transfers to real-world platforms even without domain randomization. Compared to prior work, our approach leads to very reliable training behavior and does not require the cherry-picking of trained policies. Furthermore, we conduct a large ablation study and find that our policies are competitive with classic controllers.

We open-source our approach and simulator setup to the community to democratize learning-based quadrotor control. Due to the curse of dimensionality, the design space (in terms of hyperparameters and other design decisions) of RL-based end-to-end quadrotor control is still sparsely explored and we believe that our experimental results constitute a foundation that future research can build upon. Our proposed training paradigm and the resulting highly optimized implementation allow for greatly reduced training times and hence more rapid iteration. We would also like to note that the Crazyflie quadrotor uses open-source firmware and is widely available and relatively inexpensive.

Future works will push the training speed and robustness as well as the tracking performance of learned low-level controllers through automatic hyperparameter optimization. Furthermore, we are interested in extending the policy to be adaptive to changing system or environment parameters like battery levels or wind, possibly using meta-RL.

REFERENCES

- [1] A. Krizhevsky, I. Sutskever, and G. E. Hinton, "ImageNet classification with deep convolutional neural networks," *Communications of the ACM*, vol. 60, no. 6, pp. 84–90, 2012.
- [2] K. He, X. Zhang, S. Ren, and J. Sun, "Deep Residual Learning for Image Recognition," in *IEEE Conference on Computer Vision and Pattern Recognition (CVPR)*, 2016, pp. 770–778.
- [3] V. Mnih, K. Kavukcuoglu, D. Silver, A. A. Rusu, J. Veness, M. G. Bellemare, A. Graves, M. Riedmiller, A. K. Fidjeland, G. Ostrovski, S. Petersen, C. Beattie, A. Sadik, I. Antonoglou, H. King, D. Kumaran, D. Wierstra, S. Legg, and D. Hassabis, "Human-level control through deep reinforcement learning," *Nature*, vol. 518, no. 7540, pp. 529–533, 2015.
- [4] T. P. Lillicrap, J. J. Hunt, A. Pritzel, N. Heess, T. Erez, Y. Tassa, D. Silver, and D. Wierstra, "Continuous control with deep reinforcement learning," in *International Conference on Learning Representations (ICLR)*, 2016.
- [5] J. Schulman, P. Moritz, S. Levine, M. I. Jordan, and P. Abbeel, "High-dimensional continuous control using generalized advantage estimation," in *International Conference on Learning Representations (ICLR)*, 2016.
- [6] J. Schulman, F. Wolski, P. Dhariwal, A. Radford, and O. Klimov, "Proximal Policy Optimization Algorithms," 2017.
- [7] J. Tobin, R. Fong, A. Ray, J. Schneider, W. Zaremba, and P. Abbeel, "Domain Randomization for Transferring Deep Neural Networks from Simulation to the Real World," in *IEEE/RSJ International Conference on Intelligent Robots and Systems (IROS)*, 2017, pp. 23–30.
- [8] X. B. Peng, M. Andrychowicz, W. Zaremba, and P. Abbeel, "Sim-to-Real Transfer of Robotic Control with Dynamics Randomization," in *IEEE International Conference on Robotics and Automation (ICRA)*, 2018, pp. 3803–3810.
- [9] OpenAI, I. Akkaya, M. Andrychowicz, M. Chociej, M. Litwin, B. McGrew, A. Petron, A. Paino, M. Plappert, G. Powell, R. Ribas, J. Schneider, N. Tezak, J. Tworek, P. Welinder, L. Weng, Q. Yuan, W. Zaremba, and L. Zhang, "Solving Rubik's Cube with a Robot Hand," 2019.
- [10] K. Hornik, M. Stinchcombe, and H. White, "Multilayer feedforward networks are universal approximators," *Neural Networks*, vol. 2, no. 5, pp. 359–366, 1989.
- [11] S. Kohlbrecher, J. Meyer, T. Graber, K. Petersen, U. Klingauf, and O. von Stryk, "Hector Open Source Modules for Autonomous Mapping and Navigation with Rescue Robots," in *RoboCup 2013: Robot World Cup XVII*, 2014, vol. 8371, pp. 624–631.
- [12] S. Shah, D. Dey, C. Lovett, and A. Kapoor, "AirSim: High-Fidelity Visual and Physical Simulation for Autonomous Vehicles," in *Field and Service Robotics*, 2018, vol. 5, pp. 621–635.
- [13] Y. Song, S. Naji, E. Kaufmann, A. Loquercio, and D. Scaramuzza, "Flightmare: A Flexible Quadrotor Simulator," in *Conference on Robot Learning*, 2020, pp. 1147–1157.
- [14] J. Panerati, H. Zheng, S. Zhou, J. Xu, A. Prorok, and A. P. Schoellig, "Learning to Fly - a Gym Environment with PyBullet Physics for Reinforcement Learning of Multi-agent Quadcopter Control," in *IEEE/RSJ International Conference on Intelligent Robots and Systems (IROS)*, 2021.
- [15] F. Furrer, M. Burri, M. Achtelik, and R. Siegwart, "RotorS - A Modular Gazebo MAV Simulator Framework," in *Robot Operating System (ROS): The Complete Reference (Volume 1)*, 2016.
- [16] G. Li, X. Liu, and G. Loianno, "RotorTM: A Flexible Simulator for Aerial Transportation and Manipulation," *IEEE Transactions on Robotics*, 2023.
- [17] F. Sadeghi and S. Levine, "Cad2rl: Real single-image flight without a single real image," in *Proceedings of Robotics: Science and Systems*, Cambridge, Massachusetts, 2017.
- [18] R. Polvara, M. Patachiola, S. Sharma, J. Wan, A. Manning, R. Sutton, and A. Cangelosi, "Autonomous Quadrotor Landing using Deep Reinforcement Learning," 2018.
- [19] C. Sampedro, A. Rodriguez-Ramos, I. Gil, L. Mejias, and P. Campoy, "Image-Based Visual Servoing Controller for Multirotor Aerial Robots Using Deep Reinforcement Learning," in *IEEE/RSJ International Conference on Intelligent Robots and Systems (IROS)*, 2018, pp. 979–986.
- [20] S. Belkhal, R. Li, G. Kahn, R. McAllister, R. Calandra, and S. Levine, "Model-Based Meta-Reinforcement Learning for Flight with Suspended Payloads," *IEEE Robotics and Automation Letters*, vol. 6, no. 2, pp. 1471–1478, 2021.
- [21] B. Rubí, B. Morcego, and R. Pérez, "Deep reinforcement learning for quadrotor path following with adaptive velocity," *Autonomous Robots*, vol. 45, no. 1, pp. 119–134, 2021.
- [22] E. Kaufmann, L. Bauersfeld, and D. Scaramuzza, "A Benchmark Comparison of Learned Control Policies for Agile Quadrotor Flight," in *IEEE International Conference on Robotics and Automation (ICRA)*, 2022, pp. 10 504–10 510.
- [23] P. Becker-Ehmck, M. Karl, J. Peters, and P. van der Smagt, "Learning to Fly via Deep Model-Based Reinforcement Learning," Aug. 2020.
- [24] J. Lin, L. Wang, F. Gao, S. Shen, and F. Zhang, "Flying through a narrow gap using neural network: an end-to-end planning and control approach," in *IEEE/RSJ International Conference on Intelligent Robots and Systems (IROS)*, 2019, pp. 3526–3533.
- [25] J. E. Kooi and R. Babuska, "Inclined Quadrotor Landing using Deep Reinforcement Learning," in *IEEE/RSJ International Conference on Intelligent Robots and Systems (IROS)*, 2021, pp. 2361–2368.
- [26] E. Kaufmann, A. Loquercio, R. Ranftl, M. Müller, V. Koltun, and D. Scaramuzza, "Deep Drone Acrobatics," in *Robotics: Science and Systems*, 2020.
- [27] A. Romero, Y. Song, and D. Scaramuzza, "Actor-Critic Model Predictive Control," 2023.
- [28] J. Hwangbo, I. Sa, R. Siegwart, and M. Hutter, "Control of a Quadrotor with Reinforcement Learning," *IEEE Robotics and Automation Letters*, vol. 2, no. 4, pp. 2096–2103, 2017.
- [29] A. Molchanov, T. Chen, W. Hönig, J. A. Preiss, N. Ayanian, and G. S. Sukhatme, "Sim-to-(Multi)-Real: Transfer of Low-Level Robust Control Policies to Multiple Quadrotors," in *IEEE/RSJ International Conference on Intelligent Robots and Systems (IROS)*, 2019, pp. 59–66.
- [30] C.-H. Pi, K.-C. Hu, S. Cheng, and I.-C. Wu, "Low-level autonomous control and tracking of quadrotor using reinforcement learning," *Control Engineering Practice*, vol. 95, p. 104222, 2020.
- [31] Y. Song, M. Steinweg, E. Kaufmann, and D. Scaramuzza, "Autonomous Drone Racing with Deep Reinforcement Learning," in *IEEE/RSJ International Conference on Intelligent Robots and Systems (IROS)*, 2021, pp. 1205–1212.
- [32] D. Zhang, A. Loquercio, X. Wu, A. Kumar, J. Malik, and M. W. Mueller, "Learning a Single Near-hover Position Controller for Vastly Different Quadcopters," in *IEEE International Conference on Robotics and Automation (ICRA)*, 2023, pp. 1263–1269.
- [33] W. Koch, "Flight controller synthesis via deep reinforcement learning," Ph.D. dissertation, 2019.
- [34] L. Pinto, M. Andrychowicz, P. Welinder, W. Zaremba, and P. Abbeel, "Asymmetric Actor Critic for Image-Based Robot Learning," in *Robotics: Science and Systems XIV*, 2018.
- [35] J. Eschmann, "Reward function design in reinforcement learning," *Reinforcement Learning Algorithms: Analysis and Applications*, pp. 25–33, 2021.
- [36] J. Eschmann, D. Albani, and G. Loianno, "RLtools: A Fast, Portable Deep Reinforcement Learning Library for Continuous Control," 2023.
- [37] N. O. Lambert, D. S. Drew, J. Yaconelli, S. Levine, R. Calandra, and K. S. J. Pister, "Low-Level Control of a Quadrotor With Deep Model-Based Reinforcement Learning," *IEEE Robotics and Automation Letters*, vol. 4, no. 4, pp. 4224–4230, 2019.
- [38] D. Mellinger and V. Kumar, "Minimum snap trajectory generation and control for quadrotors," in *IEEE International Conference on Robotics and Automation (ICRA)*, 2011, pp. 2520–2525.
- [39] D. Brescianini, M. Hehn, and R. D'Andrea, "Nonlinear quadcopter attitude control: Technical report," ETH Zurich, Tech. Rep., 2013.
- [40] E. J. J. Smeur, Q. Chu, and G. C. H. E. de Croon, "Adaptive Incremental Nonlinear Dynamic Inversion for Attitude Control of Micro Air Vehicles," *Journal of Guidance, Control, and Dynamics*, vol. 39, no. 3, pp. 450–461, 2016.